Multiple-spin exchange in a two-dimensional Wigner crystal

Masafumi Katano and D. S. Hirashima
Institute of Physics, University of Tsukuba, Ibaraki 305-8571, Japan
(Received 22 February 2000)

Multiple-spin exchange constants in a two-dimensional Wigner crystal are calculated with a WKB approximation. Contributions of the Gaussian fluctuations around classical exchange paths are accurately calculated. In the dilute limit, the three-spin exchange interaction is found to be dominant in agreement with the previous study. Over a wide range of the electron density, however, n-spin exchange interactions with $n \geqslant 4$ are found to be of considerable magnitude, which makes the ground phase diagram nontrivial. Recent experimental findings by Okamoto and Kawaji [Phys. Rev. B **57**, 9097 (1998)] are also discussed in the light of the present results.

I. INTRODUCTION

The importance of the multiple-spin exchange in a Wigner crystal was first pointed out by Herring[1] long ago. Later, Roger[2] calculated the multiple-spin exchange constants in a two-dimensional Wigner crystal using a WKB approximation, and found that the three-spin exchange, which is ferromagnetic, was dominant in the dilute limit. Only recently, Okamoto and Kawaji[3] succeeded in studying magnetism of a two-dimensional (2D) Wigner crystal and found that the dominance of the three-spin exchange interaction consistently explained their findings. One of the most interesting findings by Okamoto and Kawaji was that the exchange constants changed their signs, as the strength of a magnetic field perpendicular to the two-dimensional plane was changed, due to the Aharanov-Bohm (AB) effect. From this, they could estimate the multiple-spin exchange constants and the area enclosed by the exchanging particles. They found that the magnitude of the exchange constants fairly agreed with those calculated using the expressions given by Roger[2] while the results for the areas enclosed by the exchanging particles did not.

The purpose of this paper is to calculate the multiple-spin exchange constants in the 2D Wigner crystal with a WKB approximation by extending Roger's work. The extentions by the present study are (i) accurate calculation of the contribution from the Gaussian fluctuations around a classical exchange path by means of the instanton method, (ii) calculation of the five- and six-spin exchange constants, (iii) study of the size dependence of the exchange constants, and (iv) study of the effective areas enclosed not only by the exchanging particles but also by the surrounding particles. Roger could estimate only an order of magnitude of the exchange constants, because he only crudely estimated the contribution from the fluctuations around a classical exchange path. Using the standard instanton method,[4,5] it is rather straightforward to calculate the contribution of the Gaussian fluctuations. Second, there is no reason why the five-spin (or the six-spin) exchange interaction is negligibly small compared with the n-spin exchange interaction with $n \leqslant 3$, in particular when the electron density is high. Third, because the Coulomb interaction is long-ranged, the system size with which one can accurately estimate the exchange constants may be large compared with the case with solid ^{3}He. Roger used at most 18 particles which can be displaced from the equilibrium positions. It appears that the number of particles that can be displaced is not large enough to obtain an accurate estimate. Another problem is the areas enclosed by the exchange paths. The areas estimated with the WKB calculation are found to be smaller than those estimated with the experiment by Okamoto and Kawaji.[3] It is possible that, if the exchanging particles rotate clockwise, the surrounding particles are displaced from the equilibrium positions, rotate counterclockwise, and return to the equilibrium positions.[6] Then, the effective areas, which will be experimentally observed, will be reduced from the areas enclosed by the exchanging particles, and the discrepancy between the experimental estimates and the theoretical ones may be resolved.

We resort to a WKB approximation as Roger did.[2] In a clean system, a two-dimensional electron system crystallizes into a Wigner solid at $r_s \simeq 37$,[7,8] where r_s is the reduced average interparticle distance, $r_s \propto \hbar^{-2}$. In the WKB approximation, contributions of the order of $r_s^{-1/4}$ are taken into account, while those of the order of $r_s^{-1/2}$ and of higher orders are discarded. In a clean Wigner crystal, therefore, the WKB approximation works quantitatively. In the experiment by Okamoto and Kawaji, $r_s \simeq 8$;[3] electrons crystallize under the influence of impurities.[9] In this case, the results of the WKB approximation may not be quantitatively reliable. Still, an accurate WKB calculation is important in that it gives a firm reference in discussing the effect of large quantum fluctuations and other possible effects that are not considered in the calculation.

In the next section, we give the formulation for the calculation of the exchange constants, and in Sec. III, we present numerical results. Section IV is devoted to a summary and discussion. Numerical details are presented in the Appendix.

II. FORMULATION

The concept and the method of calculation of the exchange constants were discussed in the paper of Thouless.[10] As they have been frequently discussed in the literature,[2,11–13] we give a brief summary here.

We calculate the density-matrix element $\rho(X_{P(n)}, X_I; \beta)$,

$$\rho(X_{P(n)}, X_I; \beta) = \langle X_{P(n)} | e^{-\beta \mathcal{H}} | X_I \rangle, \tag{1}$$

where β is the inverse of temperature and $\mathcal{H}$ is the Hamiltonian describing the two-dimensional N-electron system. In the absence of the kinetic energy term, i.e., in the classical limit, a two-dimensional electron system forms a triangular Wigner crystal.[14,15] In this limit, the N-electron system has $N!$-fold degenerate ground states, and one of them is denoted by $|X_I\rangle$.[16] We can assume that the ith electron, whose coordinate is denoted by $\boldsymbol{r}_i$, is localized at the ith lattice site $\boldsymbol{R}_i$ in the state $|X_I\rangle$,

$$\boldsymbol{r}_i=\boldsymbol{R}_i \quad (i=1,\ldots,N). \tag{2}$$

We collectively denote the coordinates of N electrons by a $2N$-dimensional vector $\boldsymbol{X}$; $\boldsymbol{X}=(\boldsymbol{r}_1,\ldots,\boldsymbol{r}_N)$. We then rewrite Eq. (2) by

$$\boldsymbol{X}=\boldsymbol{X}_I. \tag{3}$$

The state $|X_{P^{(n)}}\rangle$ is obtained from $|X_I\rangle$ by permutating n particles with the remaining $N-n$ particles fixed. Electron coordinates are given by

$$\boldsymbol{r}_i=\boldsymbol{R}_{P(i)}, \quad (i=1,\ldots,n),$$

$$\boldsymbol{r}_j=\boldsymbol{R}_j, \quad (j=n+1,\ldots,N), \tag{4}$$

in $|X_{P^{(n)}}\rangle$, where P is an n-particle permutation operator. Alternatively, we write

$$\boldsymbol{X}=\boldsymbol{X}_{P^{(n)}}, \tag{5}$$

in $|X_{P^{(n)}}\rangle$. If the exchange rate is small compared with the Debye frequency, the density-matrix element $F(X_{P^{(n)}},X_I;\beta)$ normalized by a diagonal one is given in terms of the exchange constant J_n by[2,13,17]

$$F(X_{P^{(n)}},X_I;\beta)=\frac{\rho(X_{P^{(n)}},X_I;\beta)}{\rho(X_I,X_I;\beta)}=\tanh(\beta-\beta_P)|J_n|. \tag{6}$$

Quantity β_P is a measure of the extent to which the localized state constructed from the true ground state in the presence of the tunneling between the two cavities deviates from the state $|X\rangle$,[2,13] and corresponds to the width of the instanton (see below). If we can choose β so that $\beta_P \ll \beta \ll 1/|J_n|$,[18] Eq. (6) reduces to

$$F(X_{P^{(n)}},X_I;\beta)\simeq\beta|J_n|. \tag{7}$$

On the other hand, the density-matrix element $\rho(X_{P^{(n)}},X_I;\beta)$ is expressed with the path integral as

$$\rho(X_{P^{(n)}},X_I;\beta)=\int_{\boldsymbol{X}(0)=\boldsymbol{X}_I}^{\boldsymbol{X}(\beta)=\boldsymbol{X}_{P^{(n)}}}\mathcal{D}\boldsymbol{X}(u)\exp\{-S[\boldsymbol{X}(u)]\}, \tag{8}$$

where

$$S[\boldsymbol{X}(u)]=\sqrt{r_s}\tilde{S}[\boldsymbol{X}(u)]$$

$$=\sqrt{r_s}\int_0^\beta du\left[\frac{1}{2}\left(\frac{d\boldsymbol{X}(u)}{du}\right)^2+\frac{1}{2}\sum_{i\neq j}\frac{1}{r_{ij}}\right], \tag{9}$$

where r_s is the averaged interparticle distance r_0 normalized by the effective Bohr radius a_B^*;

$$r_s=\frac{r_0}{a_B^*}, \tag{10}$$

$$r_0=\frac{1}{\sqrt{\pi n_e}}, \tag{11}$$

and

$$a_B^*=\frac{\hbar^2}{m^*e^{*2}}, \tag{12}$$

with n_e being the electron density, m^* the electron effective mass, e^* the effective electron charge, $e^{*2}=e^2/\kappa$, and κ the dielectric constant. Here and in the following, imaginary times are in units of $[e^{*2}/(\sqrt{r_s}r_0)]^{-1}$, Coulomb energies are in units of e^{*2}/r_0, and lengths are in units of r_0, unless otherwise stated. We assume a uniform and static positive background to neutralize the system. We neglect it in Eq. (9), because it makes no contribution to the exchange constants.

In the WKB approximation, we estimate Eq. (8) by considering only the contributions from classical paths and from the Gaussian fluctuations around them. A classical path is a path which gives a minimum of the action Eq. (9),[19] and is determined by the ''equation of motion,''

$$\frac{d^2\boldsymbol{X}(u)}{du^2}=\boldsymbol{\nabla}\sum_{i<j}\frac{1}{r_{ij}}, \tag{13}$$

together with the boundary condition, $\boldsymbol{X}(0)=\boldsymbol{X}_I$ and $\boldsymbol{X}(\beta)=\boldsymbol{X}_{P^{(n)}}$. The summation on the right-hand side (rhs) is taken over the infinite range by means of the Ewald method.[20,2] Because the contribution from the classical solution $\boldsymbol{X}_0^{(n)}(u)$ to the action integral Eq. (9) is localized in imaginary time, as we see later, the solution is called an instanton. We denote the value of the action corresponding to the classical exchange path $\boldsymbol{X}_0^{(n)}(u)$ by $\tilde{S}_0^{(n)}$, and the one corresponding to the equilibrium path, $\boldsymbol{X}(u)=\boldsymbol{X}_I$, by $\tilde{S}_0^{(0)}$. Expanding the action integrals, Eq. (9), around the classical path and the equilibrium path, we have

$$F(X_{P^{(n)}},X_I;\beta)\simeq e^{-\sqrt{r_s}\Delta\tilde{S}_0^{(n)}}\frac{\int\mathcal{D}\boldsymbol{x}(u)\exp\left\{-\int_0^\beta du\,x_i(u)\left(-\delta_{ij}\frac{1}{2}\frac{d^2}{du^2}+\frac{1}{2}W_{ij}^{(n)}(u)\right)x_j(u)\right\}}{\int\mathcal{D}\boldsymbol{x}(u)\exp\left\{-\int_0^\beta du\,x_i(u)\left(-\delta_{ij}\frac{1}{2}\frac{d^2}{du^2}+\frac{1}{2}W_{ij}^{(0)}\right)x_j(u)\right\}}, \tag{14}$$

where

$$\Delta\tilde{S}_0^{(n)}=\tilde{S}_0^{(n)}-\tilde{S}_0^{(0)}, \tag{15}$$

$$W_{ij}^{(n)}(u)=\nabla_i\nabla_j\sum_{k<l}\frac{1}{r_{kl}}\bigg|_{\boldsymbol{X}(u)=\boldsymbol{X}_0^{(n)}(u)}, \tag{16}$$

$$W_{ij}^{(0)}=\nabla_i\nabla_j\sum_{k<l}\frac{1}{r_{kl}}\bigg|_{\boldsymbol{X}(u)=\boldsymbol{X}_I}, \tag{17}$$

and $\boldsymbol{x}(0)=\boldsymbol{x}(\beta)=0$. Diagonalizing the Gaussian fluctuations and denoting the eigenvalues by $\lambda_m^{(n)}$ (and $\lambda_m^{(0)}$), we have

$$F(X_{P^{(n)}},X_I;\beta)\simeq e^{-\sqrt{r_s}\Delta\tilde{S}_0^{(n)}}\prod_{m=0}\sqrt{\frac{\lambda_m^{(0)}}{\lambda_m^{(n)}}}. \tag{18}$$

At low temperatures, the lowest eigenvalue $\lambda_0^{(n)}$ is exponentially small, $\lambda_0^{(n)}\propto e^{-c\beta}$ with c being a constant,[4] and vanishes at $\beta=\infty$; the lowest eigenmode is thus called a zero mode. As the Gaussian integral becomes ill-defined, we have to treat the zero mode separately. The zero mode originates from the time translational invariance, and the contribution of the zero mode turns out to be proportional to β.[4,5,18] We thus finally have[21]

$$F(X_{P^{(n)}},X_I;\beta)\simeq\beta e^{-\sqrt{r_s}\Delta\tilde{S}_0^{(n)}}\sqrt{\frac{\sqrt{r_s}\Delta\tilde{S}_0^{(n)}\lambda_0^{(0)}}{2\pi}}\prod_{m=1}\sqrt{\frac{\lambda_m^{(0)}}{\lambda_m^{(n)}}}. \tag{19}$$

Comparing Eqs. (7) and (19), we obtain the expression for the magnitude $|J_n|$ of the n-spin exchange constant as

$$|J_n|\simeq\sqrt{\frac{\sqrt{r_s}\Delta\tilde{S}_0^{(n)}\lambda_0^{(0)}}{2\pi}}\prod_{m=1}\sqrt{\frac{\lambda_m^{(0)}}{\lambda_m^{(n)}}}e^{-\sqrt{r_s}\Delta\tilde{S}_0^{(n)}}. \tag{20}$$

Returning to ordinary energy units, we have

$$\begin{aligned}|J_n|&\simeq\frac{e^{*2}}{\sqrt{r_s}r_0}\sqrt{\frac{\sqrt{r_s}\Delta\tilde{S}_0^{(n)}\lambda_0^{(0)}}{2\pi}}\prod_{m=1}\sqrt{\frac{\lambda_m^{(0)}}{\lambda_m^{(n)}}}e^{-\sqrt{r_s}\Delta\tilde{S}_0^{(n)}}\\&=\frac{e^{*2}}{r_sa_B^*}\frac{1}{\sqrt[4]{r_s}}\sqrt{\frac{\Delta\tilde{S}_0^{(n)}\lambda_0^{(0)}}{2\pi}}\prod_{m=1}\sqrt{\frac{\lambda_m^{(0)}}{\lambda_m^{(n)}}}e^{-\sqrt{r_s}\Delta\tilde{S}_0^{(n)}}\\&\equiv\frac{e^{*2}}{a_B^*}\frac{1}{r_s}\frac{F_n}{\sqrt[4]{r_s}}e^{-\sqrt{r_s}\Delta\tilde{S}_0^{(n)}},\end{aligned} \tag{21}$$

where F_n and $\Delta\tilde{S}_0^{(n)}$ are dimensionless quantities of $O(1)$. Furthermore, we have to consider a symmetry factor A_n which takes care of the distinct paths contributing to Eq. (8);[17] $A_2=2$ and $A_n=1$ $(n=3,4,5,6)$. (The exchange path for the two-particle exchange is symmeteric with respect to $u=\beta/2$, as we see later, and consequently the symmetry factor is 2. Otherwise, it would be 4 as in the case of the two-particle exchange of high density hard core particles.[2]) The final expression for $|J_n|$ is thus

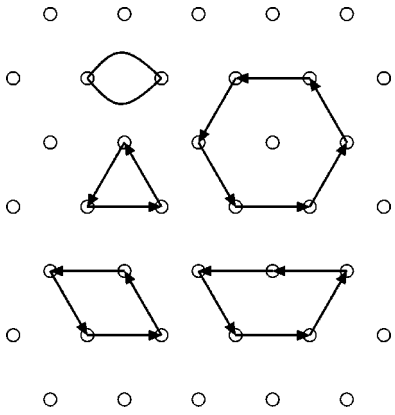

FIG. 1. Multiparticle exchange processes studied in the paper.

$$|J_n|\simeq\frac{e^{*2}}{a_B^*}\frac{1}{r_s}\frac{A_nF_n}{\sqrt[4]{r_s}}e^{-\sqrt{r_s}\Delta\tilde{S}_0^{(n)}}, \tag{22}$$

and our task is to calculate $\Delta\tilde{S}_0^{(n)}$ and F_n.

The sign of the exchange constant J_n is uniquely determined.[10] In this study, we define J_n so that $J_n<0$.

III. RESULTS

In this study, we calculate the n-spin exchange constants J_n $(n=2,\ldots,6)$. Exchange processes considered in the paper are depicted in Fig. 1. In considering an n-particle exchange process, we allow $N_{\rm tot}-n$ particles to be displaced from the equilibrium positions in addition to n exchanging particles; the total number of moving electrons is $N_{\rm tot}$. The remaining electrons are fixed at the equilibrium positions. First we allow only the nearest-neighbor electrons of the n exchanging electrons to be displaced; $N_{\rm tot}=10$ for $n=2$, for example. We then increase the number of the moving electrons by allowing the fixed electrons that are at the nearest-neighbor sites of the moving electrons to be displaced, too.

We then discretize the imaginary time interval, $0\leqslant u\leqslant\beta$, into L segments. The number of variables to be determined is thus $2N_{\rm tot}(L-1)$. We search for a solution, i.e., a classical exchange path, satisfying the equation of motion, Eq. (13), under the given boundary condition in the $2N_{\rm tot}(L-1)$-dimensional space. Once the equation is solved, the remaining task is a simple diagonalization of an $M\times M$ matrix $(M\simeq 2N_{\rm tot}L)$ representing fluctuations around the classical path.

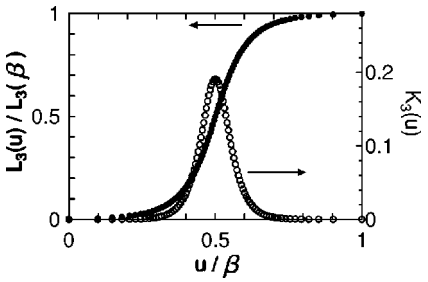

FIG. 2. Solution to the three-particle exchange problem at $\beta=30$ for $N_{\rm tot}=48$. $L_3(u)$ is the tunneling path length in the $2N_{\rm tot}$-dimensional configuration space. Kinetic energy $K_3(u)$ is also shown.

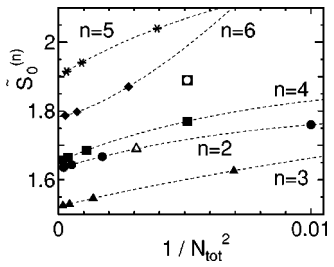

FIG. 3. Values $\tilde{S}_0^{(n)}$ of the action corresponding to the classical n-particle exchange path at $\beta=30$ for $n=2,\ldots,6$ as functions of $1/N_{\rm tot}^2$. Open symbols stand for the results by Roger (Ref. 2). Dotted curves are the results of the extrapolation.

The following results are those at $\beta=30$ and $L=64\sim90$. Further details are given in the Appendix.

A. Classical exchange paths

A typical solution is shown in Fig. 2. The path length $L_n(u)$ is defined by

$$L_n(u)=\int_0^u du\,\frac{|d\boldsymbol{X}_0^{(n)}(u)|}{du}. \tag{23}$$

The action integral $\Delta\tilde{S}_0^{(n)}$ corresponding to a classical exchange path $\boldsymbol{X}_0^{(n)}(u)$ is represented by

$$\Delta\tilde{S}_0^{(n)}=\int_0^\beta du[K_n(u)+V_n(u)]=2\int_0^\beta du K_n(u), \tag{24}$$

where

$$K_n(u)=\frac{1}{2}\left(\frac{d\boldsymbol{X}_0^{(n)}(u)}{du}\right)^2, \tag{25}$$

and $V_n(u)$ is the potential energy of the configuration $\boldsymbol{X}_0^{(n)}(u)$ (measured from the value of the equilibrium configuration). The last equality in Eq. (24) is owing to the energy conservation,[21]

$$K_n(u)=V_n(u). \tag{26}$$

As was found by Roger,[2] the trajectory is symmetric with respect to $u=\beta/2$ for any n. $K_n(u)$ is found to be well localized around $u=\beta/2$, and the particle exchange in the Wigner crystal thus makes a textbook example of a multidimensional instanton. The width β_w of the instanton is estimated from the slope of $L_n(u)$ at $u=\beta/2$. $\beta_w\simeq5$ for $n=2$, it increases as n, and $\beta_w\simeq9$ for $n=6$.

The action values $\tilde{S}_0^{(n)}$ of the n-particle exchange path for $n=2,\ldots,6$ are shown as functions of $1/N_{\rm tot}^2$ in Fig. 3. As was found by Roger,[2] the action $\tilde{S}_0^{(3)}$ of the three-particle exchange is the smallest, which means that the three-spin exchange J_3 is dominant (at least) in a dilute Wigner crystal. Roger, however, overestimated $\tilde{S}_0^{(n)}$ by 10–15 %. This is not large as it is, but can result in an underestimate of the exchange constants by a much larger factor for a large r_s. For $N_{\rm tot}\gtrsim50$, the results are well converged. In Table I, we tabulate the values of $\tilde{S}_0^{(n)}$ extrapolated to $N_{\rm tot}\to\infty$ as shown in Fig. 3.[22]

TABLE I. Parameters $\tilde{S}_0^{(n)}$ and F_n characterizing the exchange constants J_n. Values of $\tilde{S}_0^{(n)}$ are those extrapolated to $N_{\rm tot}\to\infty$ and values of F_n are those for the largest $N_{\rm tot}$, whose values are shown in parentheses, for each n.

	$\tilde{S}_0^{(n)}$	$F_n(N_{\rm tot})$
$n=2$	1.63	0.61 (70)
$n=3$	1.52	0.54 (75)
$n=4$	1.65	0.62 (80)
$n=5$	1.90	0.78 (56)
$n=6$	1.78	0.69 (61)

Other interesting quantities are the total path length $L_n(\beta)$ and the maximum value $V_n^{\max}$ of the potential along the trajectory; in the present case, $V_n^{\max}=V_n(\beta/2)=K_n(\beta/2)$.[21] If the exchange trajectory were a straight line in the $2N_{\rm tot}$-dimensional configuration space, $L_n(\beta)=\sqrt{n}a$, where a is the lattice constant. The quantity $\overline{L_n}$, defined by

$$\overline{L_n}=\frac{L_n(\beta)}{\sqrt{n}a}, \tag{27}$$

stands for the extent to which the system has to go around the potential barrier to exchange the particles. In Table II are tabulated $\overline{L_n}$ and $V_n^{\max}$ for $n=2,\ldots,6$. Obviously, both $\overline{L_2}$ and $V_2^{\max}$ are large compared with those for the more-than-two-particle exchange processes, which is why J_2 cannot be dominantly large. Using the approximation adopted by Roger,[2] a sinusoidal approximation, the action value $\tilde{S}_0^{(n)}$ can be estimated by

$$\tilde{S}_0^{(n)}\simeq\tilde{S}_{\rm sin}^{(n)}=\frac{4\sqrt{2}}{\pi}\sqrt{V_n^{\max}}L_n. \tag{28}$$

The approximated action values $\tilde{S}_{\rm sin}^{(n)}$'s are also tabulated in Table II. Except for the two-particle exchange, the sinusoidal approximation works well.

Lastly, we show the exchange paths in Figs. 4(a)–4(e). In each of the figures, the symmetry of the displacement of the particles is obvious. The surrounding particles are found to offset the area enclosed by the exchanging particles. The reduction is, however, found to be less than 5%. The total area s_n enclosed by the exchange paths is also tabulated in

TABLE II. Parameters characterizing the exchange processes: $\overline{L_n}$ is the exchange path length divided by the straight path length, $V_n^{\max}$ is the maximum of the potential energy (in units of e^{*2}/r_0) on the exchange path, $\tilde{S}_{\rm sin}^{(n)}$ is an approximate value of the action of the classical path, and s_n is the total area enclosed by the displaced particles.

	$\overline{L_n}$	$V_n^{\max}$	$\tilde{S}_{\rm sin}^{(n)}/\tilde{S}_0^{(n)}$	$s_n/(\sqrt{3}a^2/4)$
$n=2(N_{\rm tot}=70)$	1.44	0.30	1.16	0.91
$n=3(N_{\rm tot}=75)$	1.24	0.19	1.05	1.93
$n=4(N_{\rm tot}=80)$	1.18	0.18	1.04	2.94
$n=5(N_{\rm tot}=56)$	1.15	0.20	1.04	3.95
$n=6(N_{\rm tot}=61)$	1.10	0.15	1.01	6.92

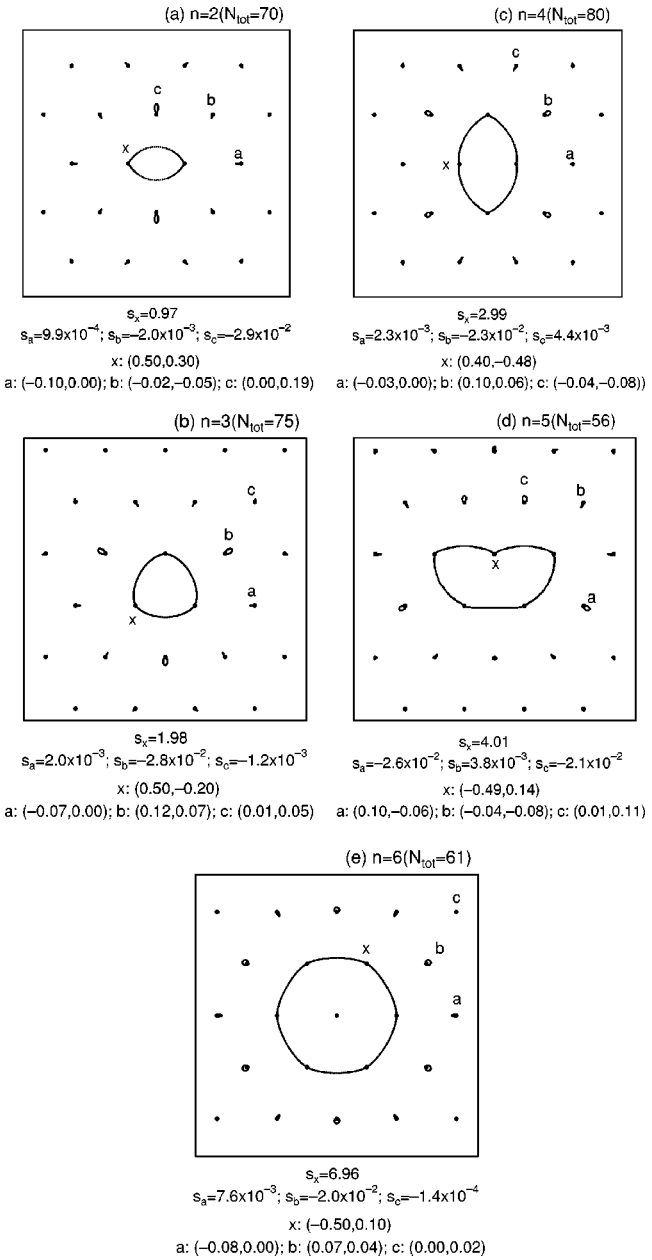

FIG. 4. Classical exchange paths for the n-particle exchange processes at $\beta=30$: (a) $n=2$, (b) $n=3$, (c) $n=4$, (d) $n=5$, and (e) $n=6$. s_x is the area enclosed by the exchanging particles, s_ν is the area enclosed by the particle denoted with ν, and they are measured in units of $3^{1/2}a^2/4$, which is the area of the equilateral triangle formed by the nearest three lattice points. The displacement vectors of particles at $u=\beta/2$ are also given.

Table II; note that the direction of the motion of each particle is considered in calculating s_n.

B. Gaussian fluctuations

The contributions F_n of the Gaussian fluctuations around the classical exchange paths are plotted as functions of $1/N_{\rm tot}$ in Fig. 5. It can be seen that F_n gets large with n. F_n's, especially those for $n=5$ and 6, do not appear to converge even for $N_{\rm tot}\gtrsim 50$, and it is difficult to extrapolate to $N_{\rm tot}\to\infty$. In Table I are thus tabulated the values of F_n calculated with the largest $N_{\rm tot}$ for each n. Obviously, those values are

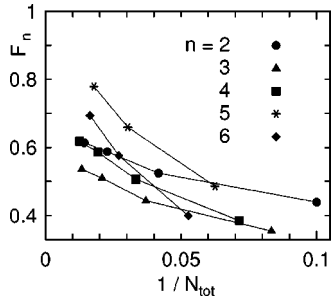

FIG. 5. Contributions F_n from the Gaussian fluctuations around the classical exchange paths for various exchange processes at $\beta=30$.

the lower bounds of F_n's. The finite-size corrections are at most 10% for $n=2$, 3, and 4, but those for $n=5$ and 6 may be larger.

C. Multiple-spin exchange constants

Using the values of $\tilde{S}_0^{(n)}$ and F_n tabulated in Table I and Eq. (21), we calculate the magnitude of the exchange constants $|J_n|$. The results are shown in Fig. 6. Clearly, the three-spin exchange J_3 is decreasing the most slowly as $r_s\to\infty$. For $r_s\lesssim 60$, however, J_3 is not necessarily dominant. Thus, in a 2D Wigner crystal, one can expect ferromagnetism owing to the three-spin exchange only in a rather dilute region. We discuss the stability of ferromagnetism in Sec. III D.

Using the values of the effective mass m^* and of the dielectric constant κ appropriate for a Si MOSFET (metal-oxide-semiconductor field-effect transistor), $m^*=0.19m$ and $\kappa=7.7$, the exchange constants in the Wigner crystal in a Si MOSFET are calculated as a function of the electron density; see Fig. 7. The result is to be compared with Fig. 11 of Ref. 3; note that J_n in Ref. 3 corresponds to $|J_n|/A_n$ in this paper. The present results and those of Ref. 3 agree qualitatively with each other. The present calculation gives larger exchange constants than Roger's, as is expected from Fig. 3. In this rather dense region, five-particle exchange processes as well as six-particle exchange processes make considerable contributions.

D. Stability of the ferromagnetic state

Now we discuss the possible magnetic states of the 2D Wigner crystal. In the absence of J_5 and J_6, the ground-state phase diagram was studied by Kubo and Momoi with a mean-field approximation.[23] Using their results, we find that

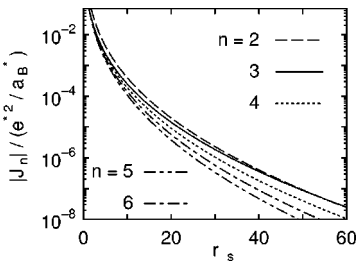

FIG. 6. Dependence of the multiple-spin exchange constants J_n in the 2D Wigner crystal on the average interparticle distance r_s.

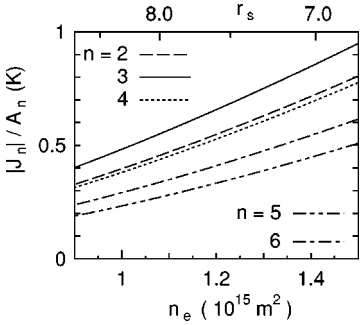

FIG. 7. Dependence of the multiple-spin exchange constants J_n (divided by the symmetry factor A_n) in the 2D Wigner crystal in a Si MOSFET on the electron density n_e.

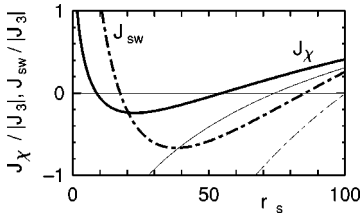

FIG. 8. J_χ, one-third of the Curie constant, and J_{sw}, coefficient of the spin-wave spectrum in a perfectly ferromagnetic state, in the 2D Wigner crystal. Thin curves stand for the results in the absence of J_5 and J_6.

the ferromagnetic state is realized only for $r_s \gtrsim 100$; the four-spin exchange interaction destabilizes the ferromagnetic state, and the ground state can have a four-sublattice structure for a smaller r_s.[24] For $30 \lesssim r_s \lesssim 100$, one of the ground states is a $uuud$ state[23,25] where three of the four-sublattice magnetizations point to the same direction and the remaining one to the opposite direction. For $r_s \lesssim 30$, the ground state is a tetrahedral state,[23] where the angle formed by any two of the four-sublattice magnetizations is θ_0 with $\cos\theta_0 = -\frac{1}{3}$.

The phase diagram can be considerably affected by the five-spin exchange and the six-spin exchange. It is quite a complicated problem, however, to determine the phase diagram in the presence of J_5 and J_6 even in a mean-field theory.[26] Here we focus on the ferromagnetic state and study its stability. The Weiss temperature Θ is given by[27]

$$\Theta = 3J_\chi = 3(J_2 - 2J_3 + 3J_4 - 5J_5 + \tfrac{5}{8}J_6). \tag{29}$$

Figure 8 shows J_χ as a function of r_s. For $r_s \gtrsim 55$, $J_\chi > 0$, implying the dominance of the ferromagnetic interaction. What is remarkable is the upturn of J_χ for $r_s \lesssim 20$ due to the five-spin exchange interaction J_5. For $J_5 = J_6 = 0$, J_χ remains negative for all $r_s \lesssim 75$. To study the stability of the perfectly ferromagnetic state, we calculate the spin-wave dispersion, and find that it is proportional to J_{sw},[28] where

$$J_{sw} = 2(J_2 - 2J_3 + 4J_4 - 10J_5 + 2J_6). \tag{30}$$

A negative J_{sw} implies an instability of the ferromagnetic state. From Fig. 8, it is found that the ferromagnetic state is unstable for $20 \lesssim r_s \lesssim 85$. For $r_s \lesssim 20$, the ferromagnetic state is stable due to J_5, while it is stable due to J_3 for $r_s \gtrsim 85$.

IV. SUMMARY AND DISCUSSION

We have calculated multiple-spin exchange constants in a 2D Wigner crystal using a WKB approximation. Taking proper account of the Gaussian fluctuations around a classical exchange path (an instanton solution), we accurately calculate the magnitude of the exchange constants within the WKB approximation. The results are summarized in Tables I and II. There are still some finite-size errors, because the contributions F_n of the Gaussian fluctuations could not be extrapolated to $N_{tot} = \infty$. Tabulated values of F_n are lower bounds; the errors are at most less than 10% for $n = 2$, 3, and 4, but may be larger for $n = 5$ and 6. The results show that the ferromagnetic interaction is dominant in the dilute region, as expected, due to the three-spin exchange interaction, and it can be also dominant in the dense region due to the five-spin exchange interaction. In the intermediate region, $20 \lesssim r_s \lesssim 85$, the perfectly ferromagnetic state cannot be the ground state.

The present results agree qualitatively with those of Roger[2] as far as the two-, three-, and four-spin exchange constants are concerned. Roger overestimated the action value $\tilde{S}_0^{(n)}$ corresponding to a classical path by 10–15 %. This does not make a large difference in J_n as far as $r_s \lesssim 10$. Values of F_n estimated by Okamoto and Kawaji using Roger's expression are also found to be in fair agreement with the present results (considering the crudeness of Roger's estimation).

Now we discuss the experimental findings by Okamoto and Kawaji[3] in the light of the present results. Their results are consistenly explained by assuming the ground state to be a ferromagnetic state. Okamoto and Kawaji estimated the magnitude of the exchange constants from the AB oscillation of the activation energy, and found $|J_2| : |J_3| : |J_4| = 1 : 1 : 0.1$ at $r_s \simeq 7.8$. These parameters are indeed consistent with a ferromagnetic ground state. The present result also shows that the ground state can be a ferromagnetic state for $r_s \simeq 8$, but it can be so only when the five-spin exchange constant is considered; the relative magnitude of J_4 is found to be rather large, $|J_2| : |J_3| : |J_4| = 1.7 : 1.0 : 0.8$ at $r_s \simeq 7.8$, in this study, and the ferromagnetic state is realized only with the help of J_5. In the experiment, however, the amplitude of rapid AB oscillations which must correspond to many-spin ($n \geqslant 4$) exchange processes was found to be small, indicating these processes did not work.[29]

Another discrepancy between the present results and the experiment is the area enclosed by the diplaced particles. Certainly, some of the surrounding particles rotate in the opposite direction to that of the exchanging particles, but the offset due to them is found to be too small to account for the small values of the area observed in the experiment.

The present theory can be improved or modified in several ways. One obvious way is to treat the quantum fluctuations more seriously, e.g., by a Monte Carlo method.[13] In the dense region where the experiment was done, the quantum fluctuations may be too large to be properly treated by the WKB approximation. Although this is definitely a worthy improvement of the theory, it may be difficult to resolve the discrepancies only by considering the fluctuations more seriously. In particular, it is unlikely that the quantum fluctuations suppress only the many-spin exchange processes severely.

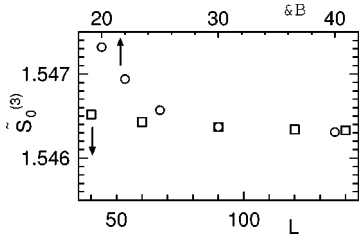

FIG. 9. $\tilde{S}_0^{(3)}$ as a function of L (open squares) and of β (open circles) at $N_{\rm tot}=27$.

Okamoto and Kawaji estimated the exchange constants from the activation energy under a magnetic field perpendicular to the 2D plane. The field, in addition to giving rise to the AB oscillation, can reduce the magnitude of the exchange constants, because a magnetic field in general helps electrons to be localized. Moreover, the area enclosed by the exchanging particles will also be changed by the field. This may partly account for the small observed values of the areas.

In the experiment, electrons crystallize with the help of impurity potentials. Impurity potentials must also affect the particle exchange processes. It is clear that the more the number of exchanging particles is, the more seriously the process is affected by impurity potentials. It is desirable to study the effect of impurities on multiple-spin exchanges.

Finally, the present calculation has assumed that electrons are strictly confined in a 2D plane. Typical Coulomb energy in the Wigner crystal in a Si MOSFET is $e^{*2}/r_0 \simeq 150$ K for $r_s \simeq 8$. The excitation energy of the first excited state in the inversion layer is around 200 K,[30] and is similar in magnitude to the typical Coulomb energy. This means the assumption of strict two-dimensionality is not so sound. If the motion in the perpendicular direction is allowed, electrons can also avoid each other in this direction, and the area enclosed by the exchange paths projected onto the plane will be reduced. This can also account for the small area enclosed by the exchanging particles observed in the experiment.

The points discussed above — (i) a fully quantum-mechanical calculation of the exchange constants in a 2D Wigner crystal, (ii) a calculation of the exchange constants in a magnetic field, (iii) study of the effect of impurities on the exchange processes, and (iv) a realistic treatment of the electrons in a Si MOSFET — certainly deserve further studies.

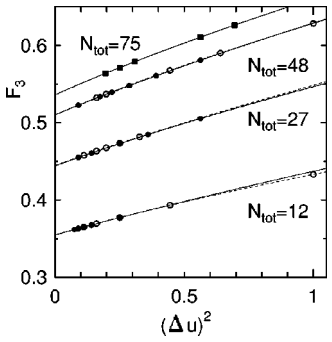

FIG. 10. F_3 for different values of $N_{\rm tot}$. Solid circles are results at $\beta=30$ and $L=90$, open circles at $\beta=40$ and $L=90$, and solid squares at $\beta=30$ and $L=64$. Solid curves represent the extrapolation of the results denoted by solid symbols, and dotted curves the results denoted by open symbols. The used formula of the extrapolation is $F_3(\Delta u)=F_3(0)+f_2(\Delta u)^2+f_3(\Delta u)^3$.

ACKNOWLEDGMENTS

We thank Kenn Kubo, T. Okamoto, T. Momoi, D. Yoshioka, and A. Tanaka for useful discussions and comments. Part of the computation in this work was done using the facilities of the Supercomputer Center, Institute for Solid State Physics. This work was supported by a Grant-in-Aid from the Ministry of Education and Science of Japan.

APPENDIX: NUMERICAL DETAILS

We minimize the reduced action $\tilde{S}[\boldsymbol{X}(u)]$,

$$\tilde{S}[\boldsymbol{X}(u)]=\int_0^\beta du\left[\frac{1}{2}\left(\frac{d\boldsymbol{X}(u)}{du}\right)^2+\frac{1}{2}\sum_{k\neq l}\frac{1}{r_{kl}}\right], \qquad \text{(A1)}$$

under a boundary condition $\boldsymbol{X}(0)=\boldsymbol{X}_I$ and $\boldsymbol{X}(\beta)=\boldsymbol{X}_{P(n)}$ by solving the equation of motion Eq. (13). The time interval, $0\leqslant u\leqslant\beta$, is discretized into L pieces. A rapid convergence can be obtained when we change the variables from u to y by

$$y=\frac{\tanh((u-\beta/2)/\beta_y)}{\tanh(\beta/(2\beta_y))} \quad (-1\leqslant y\leqslant 1) \qquad \text{(A2)}$$

and then discretize the integral region into L pieces, because the integrand in Eq. (A1) turns out to be localized around $u\simeq\beta/2$ as shown in Fig. 2. Obviously, we should take $\beta_y \simeq \beta_w$. If the temperature is not low enough, excited states with high energy (Debye frequency) contribute to the action and cause $\tilde{S}_0^{(n)}$ to be temperature dependent. We can see that β has to be much larger than the instanton width β_w for $\tilde{S}_0^{(n)}$ to become independent of β. From this we see that β_w is related to the Debye frequency. It is, however, dependent on the choice of the initial wave function $|\boldsymbol{X}_I\rangle$, too. If it were the true localized state (in the presence of the tunneling between the two cavities), then $\beta_w=0$ and we would not have to go down to low temperatures. In Fig. 9, we show the dependence of $\tilde{S}_0^{(3)}$ on β and L for $N_{\rm tot}=27$ and $\beta_y=4$; when β dependence is studied, we set $L\simeq 3\beta$, and L dependence is studied at $\beta=30$. It can be seen that $\tilde{S}_0^{(3)}$ rapidly converges as $\beta\to\infty$. It is not difficult to obtain values of $\tilde{S}_0^{(n)}$ accurate to four significant figures by calculating at $\beta\gtrsim 30$ and $L\gtrsim 60$.

Although the change of a variable, Eq. (A2), is useful in searching for the minimum of the action, it is not necessarily so for the diagonalization of the Gaussian fluctuations, because the matrix representing the fluctuations becomes asymmetric. (Numerical diagonalization of an asymmetric matrix is slightly more complicated than that of a symmetric one.) In diagonalizing the fluctuations, therefore, we return to the variable u, interpolating the classical trajectory $\boldsymbol{X}_0^{(n)}(u)$, and divide the time interval, $0\leqslant u\leqslant\beta$, into L' pieces. We show the dependence of F_3 on $\Delta u=\beta/L'$ for different values of $N_{\rm tot}$ in Fig. 10. The results are well fitted by quadratic (+cubic) polynomials. In Fig. 5 are plotted the values extrapolated to $\Delta u\to 0$.

[1] C. Herring, in *Magnetism*, edited by G.T. Rado and H. Suhl (Academic, New York, 1966), Vol. II.
[2] M. Roger, Phys. Rev. B **30**, 6432 (1984).
[3] T. Okamoto and S. Kawaji, Phys. Rev. B **57**, 9097 (1998).
[4] S. Coleman, *The Uses of Instantons*, in *Aspects of Symmetry* (Cambridge, New York, 1985).
[5] J. W. Negele and H. Orland, *Quantum Many-Particle Systems* (Addison-Wesley, New York, 1987).
[6] This possibility was pointed out by D. Yoshioka.
[7] M. Imada and M. Takahashi, J. Phys. Soc. Jpn. **53**, 3770 (1984).
[8] B. Tanatar and D.M. Ceperley, Phys. Rev. B **39**, 5005 (1989).
[9] S.T. Chui and B. Tanatar, Phys. Rev. Lett. **74**, 458 (1995).
[10] D.J. Thouless, Proc. Phys. Soc. London **86**, 893 (1965). More general discussion was also given by C. Herring, in *Magnetism*, edited by G.T. Rado and H. Suhl (Academic, New York, 1968), Vol. II.
[11] M. Roger, J.H. Hetherington, and J.M. Delrieu, Rev. Mod. Phys. **55**, 1 (1983).
[12] M.C. Cross and D.S. Fisher, Rev. Mod. Phys. **57**, 881 (1985).
[13] D.M. Ceperley and G. Jacucci, Phys. Rev. Lett. **58**, 1648 (1987).
[14] G. Meissner, H. Namaizawa, and M. Voss, Phys. Rev. B **13**, 1370 (1976).
[15] L. Bonsall and A.A. Maradudin, Phys. Rev. B **15**, 1959 (1977).
[16] In principle, we do not have to take $|X\rangle$'s as the localized states in the classical limit. We do so only because it is the simplest choice. The condition for $|X\rangle$'s is that they correspond to each one of the ''cavities'' introduced by Thouless.[10] We need not know their precise form. This is a strong merit of the present method of the calculation of the exchange constants.
[17] We should attach another suffix to J_n to distinguish various n-particle permutations, e.g., the exchange of the nearest-neighbor two particles and that of the next-nearest-neighbor two particles. In this study, we consider only one process for each n-particle exchange, and therefore we can suppress the additional suffix.
[18] In fact, the second inequality, $\beta|J_n| \ll 1$, need not be satisfied in the actual WKB calculation. It is necessary for the tunneling to occur at least once. In the present calculation, we search for a solution under a boundary condition which guarantees that the system tunnels at least once. On the other hand, when $\beta|J_n| \gg 1$ the system can experience many tunnelings (a multi-instanton solution). We can, however, simply discard more-than-one-instanton solutions to obtain only the contribution from one-instanton solutions, which is proportional to $|J_n|$. The first inequality, $\beta \gg \beta_P$, is actually necessary, but not because one can neglect β_P in Eq. (6). Considering a finite width β_w of an instanton, we see that a factor $\beta - \beta_w$ should appear in Eq. (19) instead of β. Then, we find that $\beta_P = \beta_w$, and that Eq. (20) holds even if β_P is not negligibly small compared with β. However, $\tilde{S}_0^{(n)}$ reaches a value independent of β only when $\beta \gg \beta_P$ is satisfied, as shown in the Appendix. This is why the first inequality is necessary.
[19] It is possible that there are more than one path which give minima of the action. If the values of the minima of the action are close to each other, we should take account not only of the path giving the absolute minimum but also of the other paths giving the other (local) minima in estimating Eq. (8). It is also possible that the more than one paths give the identical minimum value of the action; an example is the two-particle exchange.
[20] See, for example, C. Kittel, *Introduction to Solid State Physics* (John Wiley & Sons, New York, 1996).
[21] Use has been made of the energy conservation, $K_n(u) = V_n(u)$, Eq. (26). Strictly speaking, the conservation of energy implies that $K_n(u) - V_n(u) = \text{const}$, and the constant on the rhs vanishes only at $\beta \to \infty$. At $u = 0$ (and $u = \beta$), $V_n(u) = 0$ (note that it is measured from the equilibrium value) and $K_n(u)$ is exponentially small. The correction term at a finite β is therefore exponentially small.
[22] We assume that $\tilde{S}_0^{(n)}(N_{\text{tot}}) = \tilde{S}_0^{(n)}(\infty) + s_2 N_{\text{tot}}^{-2} + s_3 N_{\text{tot}}^{-3}$. The relative difference between the extrapolated value and the value for the maximum N_{tot} is less than 1%.
[23] K. Kubo and T. Momoi, Z. Phys. B: Condens. Matter **103**, 485 (1997).
[24] A three-sublattice structure (the so-called 120° structure) is also realized when the two-spin exchange is dominant. Using the present results, we find it is realized only when $r_s \lesssim 1$, where electrons will not crystallize.
[25] K. Kubo, T. Momoi, and K. Niki, J. Low Temp. Phys. **110**, 339 (1998).
[26] G. Misguich, B. Bernu, and C. Lhuillier, J. Low Temp. Phys. **110**, 327 (1998).
[27] B. Bernu, D. Ceperley, and C. Lhuillier, J. Low Temp. Phys. **89**, 589 (1992).
[28] M. Roger, Phys. Rev. B **56**, R2928 (1997).
[29] A small observed J_4 could be a piece of evidence of a large J_5; the five-spin exchange processes can be rewritten as a sum of pair exchange processes and four-spin exchange processes,[28] and the exchange constant for the nearest four spins is effectively reduced, $J_4 \to J_4 - 2J_5$. In the experiment,[3] however, J_4 and J_5 can be observed separately, not as a combination. Therefore, this cannot be a correct explanation of a small J_4.
[30] T. Ando, A.B. Fowler, and F. Stern, Rev. Mod. Phys. **54**, 437 (1982).